INTERNATIONAL JOURNAL FOR NUMERICAL METHODS IN FLUIDS, VOL. 24, 771–786 (1997)

# VALIDATION OF NUMERICAL SHALLOW WATER MODELS FOR STRATIFIED SEICHES

DONALD E. ELIASON

*Atmospheric Science Division, L-256, Lawrence Livermore National Laboratory PO Box 808, Livermore, CA 94551-9900, U.S.A.*

AND

ALFRED J. BOURGEOIS

*U.S. EPA MD-24/ERC-1B, Research Triangle Park, NC 27711, U.S.A.*

## SUMMARY

A new analytical solution is presented for the case of a stratified seiche. This solution, especially its energetics, is useful for the validation of numerical shallow water models under stratified conditions. The utility of the analytical solution for validation is shown by using it to validate a simple finite difference numerical model. A comparison of the energetics of the numerical and analytical solutions reveals that the model results converge rapidly to the analytical solution with increasing resolution, such that a grid size of $30 \times 30$ would appear adequate for validation. In addition to properly resolving the spatial features, good temporal resolution is also necessary for validation, i.e use of a Courant number ($Cr$) less than one. For example, owing to the numerical dispersion of the present model, using $Cr = 5/4$ rather than $Cr = 1/4$ for the $50 \times 50$ grid resulted in 3·6 times larger RMS errors of model versus analytical barotropic available potential energy.

This new analytical solution should be applied to a test suite of such validation tools before using such numerical models to simulate the more realistic geophysical flows encountered in lakes, bays, harbours and semi-enclosed seas under stratified conditions. © 1997 by John Wiley & Sons, Ltd.

KEY WORDS: shallow water equations; seiches; stratification; analytical solution; validation

## 1. INTRODUCTION

Shallow water circulation models must be numerical in order to simulate realistic geophysical flow situations, as a general analytical solution that describes the entire range of flow phenomena is intractable. For the purpose of validating such numerical models, it is necessary to have analytical solutions to the set of governing equations that the numerical models approximate. A dearth exists of analytical solutions to the equations of motion that adequately test the validity of numerical models that seek to approximate those equations. Some good examples of solutions for this purpose are given by Lynch and Officer.[1] The purpose of this paper is to provide one such analytical solution, which will be appropriate for the validation of models of the equations of motion in settings such as lakes, bays, harbours and semi-enclosed seas.



CCC 0271–2091/97/080771–16 $17.50

*Received 10 Frebruary 1995*
*Revised 15 April 1996*

The emphasis here will be on seiches. An example of a solution for a seiche in homogeneous water was given by Neumann and Pierson.[2] The presentation will proceed by first giving the equations of motion that govern seiches in closed basins. The derivation will proceed by decomposing the governing equations into their barotropic and baroclinic components and then showing their respective analytical solutions. An analysis of the energetics will be presented for both the barotropic and baroclinic components. Next, the combined solution for the (slightly simplified) governing equations will be presented. The energetics of the combined solutions will then be derived, because these integral quantities are convenient diagnostic quantities for the validity of numerical solutions. Finally, an application of the analytical solution to the validation of a simple finite difference numerical model of the governing equations will be given to illustrate the benefits of using the analytical solution to validate numerical shallow water models under stratified conditions.

## 2. GOVERNING EQUATIONS

Using the Boussinesq, hydrostatic and incompressible assumptions and neglecting the non-linear terms in the momentum equation and the horizontal advection of density in the density equation, the equations of motion that are applicable to seiche motions in a Cartesian co-ordinate, two-dimensional (length, depth) region can be simplified to

$$\frac{\partial u}{\partial t} + \frac{1}{\rho_o}\frac{\partial P}{\partial x} = 0, \tag{1}$$

$$\frac{\partial u}{\partial x} + \frac{\partial w}{\partial z} = 0, \tag{2}$$

$$\frac{\partial P}{\partial z} + \rho g = 0, \tag{3}$$

$$\frac{\partial \rho}{\partial t} + w\frac{\partial \rho}{\partial z} = 0. \tag{4}$$

Here $u$ and $w$ are velocity components in the respective $x$ (length) and $z$ (depth, positive upward) directions, $t$ is time, $g$ is the earth's gravitational acceleration, $P$ is the hydrostatic pressure and $\rho$ and $\rho_o$ are the water density and reference water density respectively.

The horizontal speed $u$ can be decomposed into a depth-averaged component $\bar{u}$ and a depth-variable component $u'$ which are defined by

$$\bar{u} = \frac{1}{H}\int_{-H}^{0} u \, dz, \tag{5}$$

where $H$ is the bottom depth, and $u' = u - \bar{u}$. With these definitions, $\bar{u}$ will correspond to the barotropic and $u'$ the baroclinic components of $u$.

 

The pressure $P$ is hydrostatic and is defined by integrating equation (3) from depth $z$ up to the perturbation of the surface, $\eta$, from mean sea level:

$$P = \int_z^\eta \rho g \, \mathrm{d}z \tag{6}$$

$$= \rho_o g\eta + \int_z^0 \rho g \, \mathrm{d}z \tag{7}$$

$$= \rho_o g\eta + \int_z^0 \bar{\rho} g \, \mathrm{d}z + \int_z^0 \rho' g \, \mathrm{d}z, \tag{8}$$

where the approximation $\int_0^\eta \rho \, \mathrm{d}z \approx \rho_o g\eta$ has been made (note that the reference density $\rho_o$ (equation (1)) is taken to be the surface density). A time-invariant linear background vertical profile of density, $\bar{\rho} = \rho_o - z\Delta\rho$, is invoked, with a corresponding constant background vertical profile of pressure, $\bar{p}$. The perturbation density $\rho'$ also has a corresponding perturbation pressure $p'$ such that $\int_{-H}^0 p' \, \mathrm{d}z = 0$.

Using the definitions for pressure and surface elevation and denoting the internal pressure as $p = \bar{p} + p'$, the momentum equation (1) can be expanded to

$$\frac{\partial u}{\partial t} + g\frac{\partial \eta}{\partial x} + \frac{1}{\rho_o}\frac{\partial p'}{\partial x} = 0, \tag{9}$$

where use has been made of the fact that $\partial\bar{p}/\partial x = 0$.

## 3. BAROTROPIC AND BAROCLINIC MODES

Equation (9) can be separated into depth-averaged (barotropic) and depth-variable (baroclinic) parts ($\bar{u}$ and $u'$). The analysis will proceed by deriving the governing equations for first the barotropic and then the baroclinic modes of the governing equations. The solutions for both modes will be given, then recombined to show the full solution.

### *3.1. Barotropic mode*

Applying the depth averaging (as in equation (5)) to equations (2) and (9) yields expressions for the evolution of the depth-averaged horizontal speed and surface elevation:

$$\frac{\partial \bar{u}}{\partial t} + g\frac{\partial \eta}{\partial x} = 0, \tag{10}$$

$$\frac{\partial \eta}{\partial t} + H\frac{\partial \bar{u}}{\partial x} = 0, \tag{11}$$

where use has been made of the definition $w(z = 0) = \partial\eta/\partial t$ to derive equation (11) and the boundary condition on $w$ for a flat bottom, $w(z = -H) = 0$. It may be noted that the depth-averaged equations are an example of the shallow water equations.

The vertical speed that corresponds to the depth-averaged system will be denoted as $\bar{w}$ and is given by the constraint that it must obey continuity:

$$\frac{\partial \bar{u}}{\partial x} + \frac{\partial \bar{w}}{\partial z} = 0. \tag{12}$$

 

These three equations (10)–(12) comprise the governing equations for the depth-averaged system. A solution to this system of equations for a seiche in a closed basin of length $L$ is[2]

$$\eta = \eta_o \cos\left(\frac{\pi x}{L}\right) \cos\left(\frac{\pi}{L} c_o t\right), \tag{13}$$

$$\bar{u} = \frac{\eta_o c_o}{H} \sin\left(\frac{\pi x}{L}\right) \sin\left(\frac{\pi}{L} c_o t\right), \tag{14}$$

$$\bar{w} = -\eta_o \frac{\pi c_o (z+H)}{LH} \cos\left(\frac{\pi x}{L}\right) \sin\left(\frac{\pi}{L} c_o t\right), \tag{15}$$

where $\eta_o$ is the amplitude of the surface elevation and $c_o$ is the gravity wave speed, $c_o = \sqrt{(gH)}$.

*3.1.1. Energetics.* The following analysis of the energetics of the barotropic mode follows quite closely Gill's[3] analysis of the energetics for shallow water motion.

The energy equations for the barotropic mode can be derived directly from equations (10) and (11). The total energy equation for the barotropic mode is obtained by multiplying equation (10) by $\rho_o H \bar{u}$ and equation (11) by $\rho_o g \eta$, then adding the two together:

$$\frac{\partial}{\partial t}(\tfrac{1}{2}\rho_o H \bar{u}^2 + \tfrac{1}{2}\rho_o g \eta^2) + \frac{\partial}{\partial x}(\rho_o g H \bar{u} \eta) = 0. \tag{16}$$

In equation (16) the quantity $\frac{1}{2}\rho_o H \bar{u}^2$ is the barotropic kinetic energy per unit area and $\frac{1}{2}\rho_o g \eta^2$ is the barotropic potential energy, per unit area, of the perturbation.

The integral of equation (16) over the length of the basin gives the total perturbation energy balance equation for the barotropic case as

$$\frac{\mathrm{d}\bar{E}}{\mathrm{d}t} + \bar{F}(x=0,t) + \bar{F}(x=L,t) = 0, \tag{17}$$

where

$$\bar{E} = \int_0^L (\tfrac{1}{2}\rho_o H \bar{u}^2 + \tfrac{1}{2}\rho_o g \eta^2)\, \mathrm{d}x = \overline{KE} + \overline{APE} \tag{18}$$

is the total barotropic perturbation energy per unit length, $\overline{KE}$ and $\overline{APE}$ are the barotropic kinetic and available potential perturbation energies respectively, and

$$\bar{F}(x,t) = \rho_o g H \bar{u} \eta \tag{19}$$

is the barotropic perturbation energy flux.

Because of the boundary conditions on $\bar{u}$ in the closed basin, $\bar{F}(x=0,t) = \bar{F}(x=L,t) = 0$. Thus the total barotropic perturbation energy $\bar{E}$ does not change with time. For the seiche solution, (13)–(15), it is easily verified that $\mathrm{d}\bar{E}/\mathrm{d}t = 0$, as

$$\overline{KE} = \tfrac{1}{4} g \rho_o \eta_o^2 L \sin^2\left(\frac{\pi}{L} c_o t\right) \tag{20}$$

and

$$\overline{APE} = \tfrac{1}{4} g \rho_o \eta_o^2 L \cos^2\left(\frac{\pi}{L} c_o t\right) \tag{21}$$

for that system. Note that $\bar{E}$ is time-invariant, because $\overline{KE}$ and $\overline{APE}$ are 90° out of phase.

### *3.2. Baroclinic mode*

The baroclinic (depth-variable) equations are derived by subtracting the barotropic equations (10)–(12) from the full system of equations. For example, the equation for the baroclinic horizontal speed

 

$u'$ is obtained by subtracting equation (10) from equation (9). The resulting set of equations for the baroclinic mode is

$$\frac{\partial u'}{\partial t} + \frac{1}{\rho_o}\frac{\partial p'}{\partial x} = 0, \tag{22}$$

$$\frac{\partial u'}{\partial x} + \frac{\partial w'}{\partial z} = 0, \tag{23}$$

$$\frac{\partial p'}{\partial z} + \rho' g = 0, \tag{24}$$

$$\frac{\partial \rho'}{\partial t} + w' \frac{\partial \bar{\rho}}{\partial z} = 0. \tag{25}$$

Equation (25) has been derived by involving the time invariance of $\bar{\rho}$ and by linearizing the density advection term (i.e. $w'\partial\bar{\rho}/\partial z$ instead of $w\partial\rho/\partial z$ in equation (4)). The non-linear effects that arise from the vertical density advection can be important and their understanding is desirable. However, the linearized model allows for an analytical solution which can be used as a validation tool for numerical models of stratified shallow water systems, which is the primary goal of the present study. Thus the important question of how to best validate the non-linear vertical density advection has been left to other studies.

A solution to the baroclinic set of equations (22)–(25) has been derived by Klinck (personal communication):

$$u' = u_o \sin\left(\frac{l\pi x}{L}\right)\cos\left(\frac{m\pi z}{H}\right)\sin(\omega t), \tag{26}$$

$$w' = -\frac{lH}{mL}u_o \cos\left(\frac{l\pi x}{L}\right)\sin\left(\frac{m\pi z}{H}\right)\sin(\omega t), \tag{27}$$

$$\rho' = \frac{m\pi P_o}{gH}\cos\left(\frac{l\pi x}{L}\right)\sin\left(\frac{m\pi z}{H}\right)\cos(\omega t), \tag{28}$$

$$p' = P_o \cos\left(\frac{l\pi x}{L}\right)\cos\left(\frac{m\pi z}{H}\right)\cos(\omega t), \tag{29}$$

were $u_o = m\pi P_o/(\rho_o NH)$ is the amplitude of the baroclinic horizontal speed, $l$ and $m$ are the horizontal and vertical mode numbers respectively, $\omega$ is the frequency of the baroclinic mode, $\omega = lHN/(mL)$, $P_o$ is the amplitude of the internal pressure perturbation and $N$ is the constant background Brunt-Väisäla frequency, $N^2 = -(g/\rho_o)\partial\bar{\rho}/\partial z$.

To ensure that the solution for the perturbation internal pressure, equation (29), obeys the integral form of the hydrostatic equation, the definition of $p'$ becomes $p' = p^o + p^*$, where the artefact $p^o$ is defined as $p^o = P_o \cos(l\pi x/L)\cos(\omega t)$ and $p^*$ is an intermediate variable, $p^* = \int_z^0 \rho' g \, dz$. The corresponding definition for $\bar{p}$ is the more straightforward $\bar{p} = \int_z^0 \bar{\rho} g \, dz$, which was used with equation (3) to produce equation (24).

*3.2.1. Energetics.* Gill[3] gives an analysis of the energetics of internal waves, which is followed closely in the following analysis of the energetics of the baroclinic mode.

 

The baroclinic perturbation energy equation is obtained by multiplying equation (22) by $\rho_o u'$, equation (23) by $p'$, equation (24) by $w'$ and equation (25) by $g^2\rho'/(\rho_o N^2)$ and adding the results:

$$\frac{\partial}{\partial t}\left(\tfrac{1}{2}\rho_o u'^2 + \frac{1}{2}\frac{g^2}{\rho_o N^2}\rho'^2\right) + \frac{\partial(u'p')}{\partial x} + \frac{\partial(w'p')}{\partial z} = 0. \tag{30}$$

The two terms of the baroclinic perturbation energy in equation (30) can be identified as the kinetic energy ($\frac{1}{2}g^2\rho_o u'^2$) and potential energy ($\frac{1}{2}g^2\rho'^2/(\rho_o N^2)$) terms. The remaining terms together are the baroclinic perturbation energy flux.

Integrating equation (30) over the area of the basin shows that the rate of change in energy over that area is equal to the flux of energy across the sides:

$$\frac{\mathrm{d}E'}{\mathrm{d}t} + F'(x=0,z,t) + F'(x=L,z,t) + F'(x,z=-H,t) + F'(x,z=0,t) = 0, \tag{31}$$

where $E'$, the total baroclinic perturbation energy per unit length, is

$$E' = \int_{-H}^{0}\int_{0}^{L}\left(\tfrac{1}{2}\rho_o u'^2 + \frac{1}{2}\frac{g^2}{\rho_o N^2}\rho'^2\right)\mathrm{d}x\,\mathrm{d}z = KE' + APE', \tag{32}$$

$KE'$ and $APE'$ are the baroclinic kinetic and available potential energies respectively and $F'(x,z,t) = u'p' + w'p'$ is the baroclinic perturbation energy flux. As in the barotropic mode, because of the boundary conditions, $F' = 0$ at the boundaries of the basin. Thus the total baroclinic perturbation energy remains constant in time. From the seiche solution for the baroclinic mode, equations (26)–(29), the baroclinic kinetic energy and baroclinic available potential energy are

$$KE' = \frac{\rho_o HLu_o^2}{8}\sin^2(\omega t), \qquad APE' = \frac{\rho_o HLu_o^2}{8}\cos^2(\omega t). \tag{33}$$

As for the barotropic energy, $E'$ does not change with time, because $KE'$ and $APE'$ are 90° out of phase.

## 4. COMBINED SOLUTION

The combined solution, which solves equations (1)–(4), except with the linearization of the density advection term, can be constructed from the above as

$$\eta = \eta_o \cos\left(\frac{\pi x}{L}\right)\cos\left(\frac{\pi}{L}c_o t\right), \tag{34}$$

$$u = \frac{\eta_o c_o}{H}\sin\left(\frac{\pi x}{L}\right)\sin\left(\frac{\pi}{L}c_o t\right) + u_o \sin\left(\frac{l\pi x}{L}\right)\cos\left(\frac{m\pi z}{H}\right)\sin(\omega t), \tag{35}$$

$$w = -\eta_o \frac{\pi c_o(z+H)}{LH}\cos\left(\frac{\pi x}{L}\right)\sin\left(\frac{\pi}{L}c_o t\right) - \frac{lH}{mL}u_o \cos\left(\frac{l\pi x}{L}\right)\sin\left(\frac{m\pi z}{H}\right)\sin(\omega t), \tag{36}$$

$$P = \rho_o g\eta + \left(\frac{\Delta\rho}{2}z^2 - \rho_o z\right)g + P_o \cos\left(\frac{l\pi x}{L}\right)\cos\left(\frac{m\pi z}{H}\right)\cos(\omega t), \tag{37}$$

$$\rho = \rho_o - z\Delta\rho + \frac{m\pi P_o}{gH}\cos\left(\frac{l\pi x}{L}\right)\sin\left(\frac{m\pi z}{H}\right)\cos(\omega t). \tag{38}$$

 

### 4.1. Energetics

Neither the barotropic nor the baroclinic total perturbation energy varies with time, so the total perturbation energy $E$ of the combined solution is also time-invariant:

$$\begin{aligned} E &= \overline{KE} + \overline{APE} + KE' + APE' \\ &= \tfrac{1}{4} g \rho_o \eta_o^2 L \sin^2\left(\frac{\pi}{L} c_o t\right) + \tfrac{1}{4} g \rho_o \eta_o^2 L \cos^2\left(\frac{\pi}{L} c_o t\right) + \frac{\rho_o H L u_o^2}{8} \sin^2(\omega t) + \frac{\rho_o H L u_o^2}{8} \cos^2(\omega t) \\ &= \frac{\rho_o L}{4} (g \eta_o^2 + \tfrac{1}{2} H u_o^2). \end{aligned} \tag{39}$$

These integral quantities should be convenient diagnostic quantities for the validity of numerical solutions of stratified seiches.

## 5. APPLICATION

In this section a simple numerical scheme using finite differences will be presented that attempts to solve the governing equations for seiches in closed basins (equations (1)–(4)). The results of the model will be compared with the analytical solution as derived above in order to show the usefulness of the analytical solution (especially the energetics) in validating such numerical models.

### 5.1. Numerical model

The barotropic mode of the numerical model is solved semi-implicitly:

$$U_i^{n+1} + \frac{gH\Delta t}{2\Delta x} (\eta_{i+1/2}^{n+1} - \eta_{i-1/2}^{n+1}) = U_i^{n-1} - \frac{gH\Delta t}{2\Delta x} (\eta_{i+1/2}^{n-1} - \eta_{i-1/2}^{n-1}), \tag{40}$$

$$\eta_i^{n+1} + \frac{\Delta t}{2\Delta x} (U_{i+1/2}^{n+1} - U_{i-1/2}^{n+1}) = \eta_i^{n-1} - \frac{\Delta t}{2\Delta x} (U_{i+1/2}^{n-1} - U_{i-1/2}^{n-1}), \tag{41}$$

where $U = H\bar{u}$ is the transport per unit width in the $x$-direction, $2\Delta t$ is the time step from time level $n-1$ to $n+1$ and $2\Delta x$ is the horizontal spatial interval between like variables on the space-staggered Arakawa 'C' grid, which are indexed by integer values of $i$, whereas variable separated only by $\Delta x$ are indexed by half-integer values of $i$. The indexing proceeds from $i = 1$ at $x = 0$ to $i = i_{\max}$ at $x = L$.

The combined simultaneous equations (40) and (41) form a tridiagonal system that is solved using what is sometimes referred to at the 'Thomas algorithm'.[4]

Upon solution of the barotropic mode equations, the baroclinic mode equations are advanced using the leapfrog method:

$$u_{i,k}^{n+1} = u_{i,k}^{n-1} - \frac{g\Delta t}{2\Delta x} (\eta_{i+1/2}^{n+1} - \eta_{i-1/2}^{n+1} + \eta_{i+1/2}^{n-1} - \eta_{i-1/2}^{n-1}) - \frac{\Delta t}{\rho_o \Delta x} (p'^n_{i+1/2,k} - p'^n_{i-1/2,k}), \tag{42}$$

$$u'^{n+1}_{i,k} = u_{i,k}^{n+1} - U_i^{n+1}/H, \tag{43}$$

$$w'^{n+1}_{i,k} = w'^{n+1}_{i,k+1} + w'^{n-1}_{i,k+1} - w'^{n-1}_{i,k} - \frac{\Delta z}{\Delta x} (u'^{n+1}_{i+1/2,k+1/2} - u'^{n+1}_{i-1/2,k+1/2} + u'^{n-1}_{i+1/2,k+1/2} - u'^{n-1}_{i-1/2,k+1/2}), \tag{44}$$

 

$$\rho'^{n+1}_{i,k} = \rho'^{n-1}_{i,k} - \frac{\Delta t}{2\Delta z}(w'^{n}_{i,k-1/2} + w'^{n}_{i,k+1/2})(\bar{\rho}_{k-1} - \bar{\rho}_{k+1}), \tag{45}$$

$$p^{*}_{i,k} = p^{*}_{i,k-1} + g\Delta z(\rho'^{n+1}_{i,k-1} + \rho'^{n+1}_{i,k}), \tag{46}$$

$$p^{o}_{i} = (p^{*}_{i,k_{max}-1} - 3p^{*}_{i,k_{max}})/4, \tag{47}$$

$$p'^{n+1}_{i,k} = p^{o}_{i} + p^{*}_{i,k}, \tag{48}$$

where $2\Delta z$ is the vertical spatial interval between like variables, indexed at integer values of $k$, and unlike variables are at the half-integer values (e.g. $k + \frac{1}{2}$). Except for the continuity equation (44) and the first two pressure equations (46) and (47) the baroclinic equations are computed from $k = 1$ to $k = k_{max}$, while all equations are computed from $i = 1$ to $i = i_{max}$.

Note that the continuity equation (44) from which $w'$ is computed is averaged over time levels $n - 1$ and $n + 1$, as is its barotropic analogue (41), and that it is integrated upwards from the bottom boundary condition of $w' = 0$ at $z = -H$ ($k = k_{max}$) to the mean sea surface at $z = 0$ ($k = 1$).

To begin the vertical integration for the intermediate variable $p^{*}_{i,k}$ at $k = 1$, it is estimated as $p^{*}_{i,1} = g\rho'^{n+1}_{i,1}\Delta z/2$, after which equation (46) is integrated from $k = 2$ to $k = k_{max}$. Subsequently, the pressure artefact $p^{o}_{i}$ is computed from equation (47), which is derived by noting that $p^{o} = -\frac{1}{2}p^{*}(z = -H)$ and using linear extrapolation to estimate $p^{*}(z = -H)$ from the two pressure points nearest to the bottom.

The numerical model is applied to a basin with dimensions and stratification similar to those of East Lagoon, a narrow and shallow coastal lagoon in Galveston, Texas (Figure 1). The dimensions of East Lagoon are $L = 2$ km in length and a maximum of $H = 5$ m in depth. It has a summertime stratification in the deeper landward basin that can vary from $\rho_o = 1021$ kg m$^{-3}$ at the surface to $\rho_H = 1023$ kg m$^{-3}$ in the bottom of the basin. With these parameter values the barotropic seiche period is $\bar{T} = 2L/c_o = 9{\cdot}52$ min and the baroclinic seiche period for the first vertical and horizontal modes ($l = m = 1$) is $T' = 2\pi/\omega = 11{\cdot}26$ h. The model was run with a spatial resolution of $\Delta x = 20$ m and $\Delta z = 0{\cdot}05$ m, resulting in a grid size of $50 \times 50$ density points.

The initial conditions for the numerical model were set by specifying the solutions at time $t = 0$ of the barotropic (equations (13)–(15)) and baroclinic (equations (26)–(29)) modes on the East Lagoon grid points. The parameters for the initial conditions were specified using the above density stratification, and $\eta_o = 5$ cm and $u_o = 10$ cm s$^{-1}$.

To determine the effects of using less resolution, four additional 'long' runs were also made, as summarized in Table I. Also, one more run was done using the $50 \times 50$ grid, but using the same time step as the $10 \times 10$ grid, to determine the effect of using a larger time step.

The energetics of all of these runs were compared with the energetics of the analytical solution by computing the root mean square error (RMSE) and the index of agreement, $d$ (which Wilmott[6] has argued is preferable to the correlation coefficient for model validation):

$$d = 1 - \frac{\sum_{n=1}^{n_{max}} (A_n - N_n)^2}{\sum_{n=1}^{n_{max}} (|A'_n| + |N'_n|)^2} \tag{49}$$

where $A_n$ are the analytical energetics (e.g. $\overline{APE}$), $N_n$ are the numerical energetics, $A'_n = A_n - \bar{A}$ and $N'_n = N_n - \bar{A}$ with $\bar{A}$ being the mean of the analytical energetics. The interpretation of the index of

 

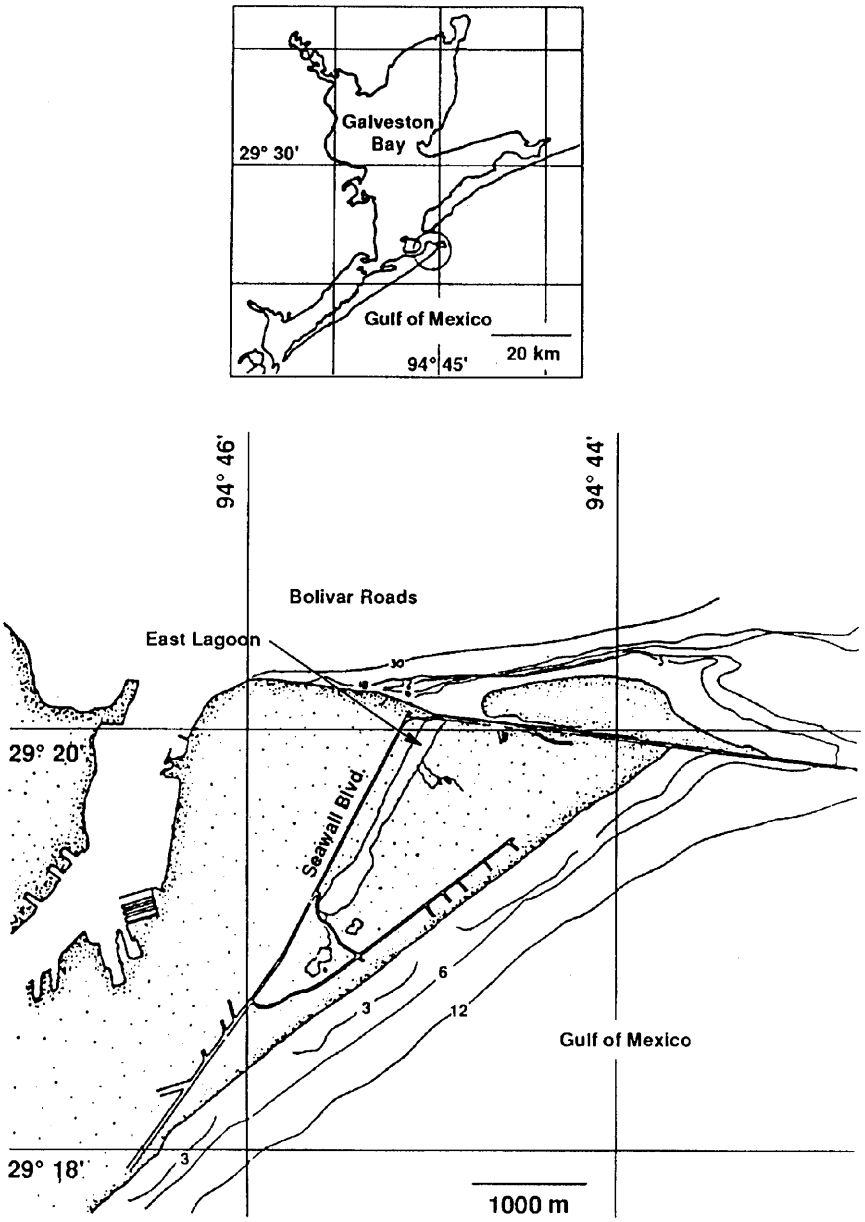


Figure 1. Geographical location of East Lagoon on Galveston Island, Texas (after Livingston[5])

agreement, which has a range of $0 \leqslant d \leqslant 1$, is that values of $d$ which are close to unity indicate that the model results agree very well with the analytical solution, while value of $d$ which are close to zero indicate poor agreement of the model results with the analytical solution. In a loose way, one can think of the RMS error as being a measure of how well the model results agree with the analytical solution in terms of magnitude, and $d$ as being a measure of how well the pattern of the model results matches the pattern of the analytical solution.

 

Table I. Grid sizes (number of density points), corresponding grid interval sizes (in metres) and time steps (in seconds) for five runs that were done to test effects of changing resolution and one additional run that was done to test effect of increasing time step (the 50 × 50† grid)

| Grid | $\Delta x$(m) | $\Delta z$(m) | $\Delta t$(s) |
|---|---|---|---|
| 10 × 10 | 100 | 0·25 | 3·52 |
| 20 × 20 | 50 | 0·12$\bar{5}$ | 1·76 |
| 30 × 30 | 33·$\bar{3}$ | 0·08$\bar{3}$ | 1·17 |
| 40 × 40 | 25 | 0·0625 | 0·88 |
| 50 × 50 | 20 | 0·05 | 0·70 |
| 50 × 50† | 20 | 0·05 | 3·52 |

For the 50 × 50 grid a time step of $\overline{\Delta t} = \bar{T}/640 \approx 0{\cdot}892$ s was used for the 'short' run to $n = n_{\max} = 640$ to illustrate the barotropic response and a time step of $\Delta t' = T'/57600 \approx 0{\cdot}704$ s was used for the 'long' run to $n_{\max} = 57{,}600$ to show the baroclinic response. As shown in Table I, the time steps were varied proportionally to the grid interval sizes for the coarser resolution cases.

An explicit time step was used to step the solution forwards from the initial conditions to the first time step. A 1–2–1 temporal smoother suggested by Killworth[7] was used to couple the two modes that resulted from this start-up procedure, to damp out the computational mode exhibited by the leapfrog scheme.[8] The temporal smoother was subsequently applied every 30th time step.

### 5.2. *Results*

A visual comparison of the numerical with the analytical energetics for both one period of the barotropic mode (the 'short run', Figure 2) and one period of the baroclinic mode (the 'long run', Figure 3) shows that the energetics of the numerical results agree quite well with the analytical solution. Small variations in the numerical results from the analytical solution due to the computational mode of the leapfrog scheme are efficiently damped by the temporal smoother.

The total energy, as expressed in equation (39), is constant in time. Integration of the equations for density shows that the basin integral of $\rho'$ is zero, so the only contribution to the total mass comes from the background density profile, whose basin integral is $HL(\rho_o + \rho_H)/2$. Figure 4, which shows these quantities versus time for both the analytical and the numerical solution, demonstrates that the numerical model conserves both mass and total energy well.

The results of varying the resolution (as summarized in Table II) show that the model results converge quickly to the analytical solution for the energetics as the resolution increases. The RMSE decreases with increasing resolution and the index of agreement increases. Figure 5 shows that the RMSE decreases exponentially with linearly increasing resolution, while the index of agreement only increases exponentially for the barotropic mode (plots for *KE* were nearly identical with those for *APE*). In contrast, high values ($d > 0{\cdot}97$) were obtained for the index of agreement for the baroclinic mode for all resolutions that were run.

The results of the final run that was done using the 50 × 50† grid were that the barotropic mode energetics were much worse in comparison with the analytical solution than those using the 50 × 50 grid, but the baroclinic mode energetics agreed with the analytical solution just about as well. As shown in Table II, increasing the time step to five times its previous size had the result of increasing the RMSE from 0·42 to 1·5 kJ m$^{-1}$ (i.e. 3·6 times larger) while decreasing the index of agreement from 0·998 to 0·970. It will be shown in Section 5·3 that this decrease in how well the model results agree with the analytical barotropic energetics, without a corresponding decrease in the agreement in

 

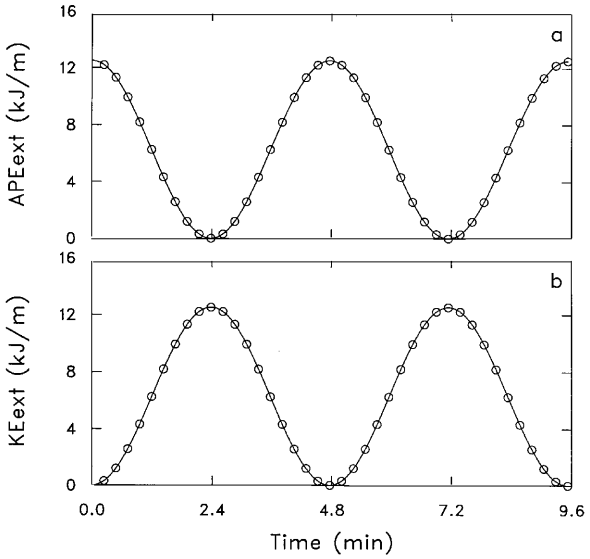


Figure 2. Energetics of analytical (circles) and 50 × 50 grid numerical (full line) solutions for one period of barotropic seiche: a, available potential energy of barotropic mode (APEext = $\overline{APE}$); b, kinetic energy (KEext = $\overline{KE}$)

the baroclinic energetics, is due to the numerical dispersion of the semi-implicit solution of the barotropic mode.

### 5.3. *Discussion*

The statistical measures given in Table II and shown in Figure 5 reflect the fact that at lower spatial resolutions the numerical barotropic mode gets out of phase with the analytical solution. Figure 6 illustrates this phase shift for the last barotropic mode of the run using the 10 × 10 grid. The very low

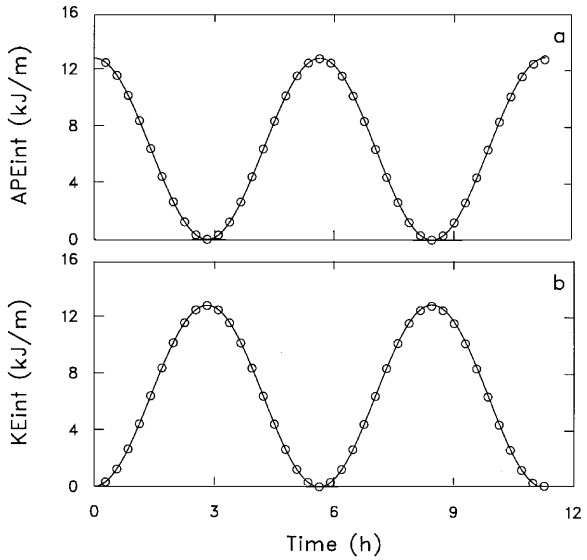


Figure 3. Energetics of analytical (circles) and 50 × 50 grid numerical (full line) solutions for one period of baroclinic seiche: a, available potential energy of baroclinic mode (APEint = $APE'$); b, kinetic energy (KEint = $KE'$)

 

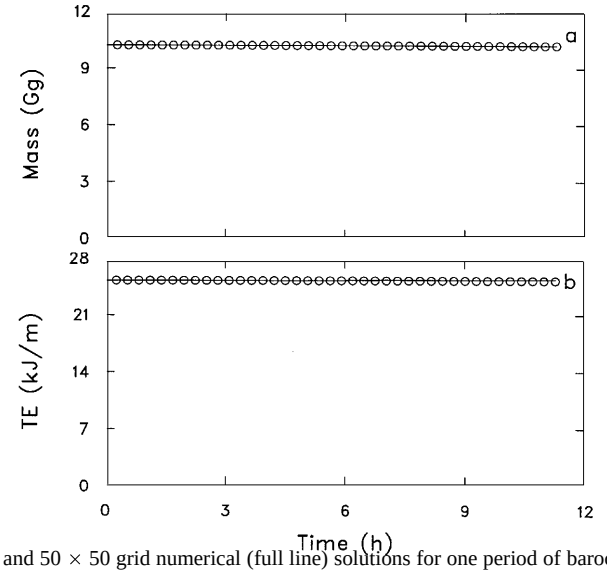


Figure 4. Analytical (circles) and 50 × 50 grid numerical (full line) solutions for one period of baroclinic seiche: a, total mass; b, total energy. Note that both quantities are well conserved by the numerical model

values of $d$ obtained for the 10 × 10 grid support the interpolation of $d$ as an indicator of how well the model results match the pattern of the analytical solution. The relatively high RMSE obtained for that solution was primarily because of the phase shift; the magnitude of the numerical $\overline{APE}$ was otherwise quite close to the analytical values (Figure 6).

In contrast with the index of agreement for $\overline{APE}$, $d$ remained high for $APE'$ regardless of the grid resolution, because the baroclinic period was so much more well resolved in time than was the barotropic period. For example, the time step used for the 10 × 10 grid resulted in only 162 time steps per barotropic period versus 11,520 per baroclinic period, while for the 50 × 50 grid 811 time steps were made per barotropic period versus 57,600 per baroclinic period.

One might be tempted to conclude that the mismatch in the phase of the numerical versus analytical $\overline{APE}$ and $\overline{KE}$ in the lower-resolution cases was due to numerical dispersion. After all, as shown in the Appendix, the semi-implicit portion of the numerical scheme is dispersive. However, the numerical dispersion is dependent upon the Courant number (see equation (55) in the Appendix). Because the time step for the varying resolution runs was varied proportionally to the grid interval size (Table I), the Courant number remained the same ($Cr = 1/4$). Only the run using the 50 × 50† grid used a different Courant number ($Cr = 5/4$). As can be seen from Figure 7 in the Appendix, the dispersion for the run using the 50 × 50† grid was much greater than that for the run using the 50 × 50 grid. This larger numerical dispersion was responsible for the worsening of agreement between the numerical results and the analytical solution for the barotropic energetics, without any corresponding decrease in the agreement for the baroclinic energetics, when going from the 50 × 50 to the 50 × 50† grid.

## 6. CONCLUSIONS

An analytical solution has been presented for the case of a stratified seiche. The analytical solution is useful for the validation of numerical shallow water models under stratified conditions, especially the energetics of the solution. As an example, a simple finite difference model of the governing equations

 

Table II. Root mean square error (RMSE) and index of agreement, *d*, for comparison of model energetics results with analytical solution for five different grid resolutions. The 50 × 50† grid denotes the 50 × 50 grid, but using the time step of the 10 × 10 grid (see Table I)

| Grid | Quantity | RMSE (kJ $m^{-1}$) | *d* |
|---|---|---|---|
| 10 × 10 | $\overline{APE}$ | 6·8 | 0·345 |
| | $\overline{KE}$ | 6·8 | 0·345 |
| | $APE'$ | 1·1 | 0·987 |
| | $KE'$ | 1·5 | 0·975 |
| 20 × 20 | $\overline{APE}$ | 2·6 | 0·911 |
| | $\overline{KE}$ | 2·6 | 0·911 |
| | $APE'$ | 0·27 | 0·999 |
| | $KE'$ | 0·35 | 0·998 |
| 30 × 30 | $\overline{APE}$ | 1·2 | 0·982 |
| | $\overline{KE}$ | 1·2 | 0·982 |
| | APE′ | 0·12 | 1·000 |
| | KE′ | 0·15 | 1·000 |
| 40 × 40 | $\overline{APE}$ | 0·66 | 0·994 |
| | $\overline{KE}$ | 0·66 | 0·994 |
| | $APE'$ | 0·068 | 1·000 |
| | $KE'$ | 0·085 | 1·000 |
| 50 × 50 | $\overline{APE}$ | 0·42 | 0·998 |
| | $\overline{KE}$ | 0·42 | 0·998 |
| | $APE'$ | 0·043 | 1·000 |
| | $KE'$ | 0·054 | 1·000 |
| 50 × 50† | $\overline{APE}$ | 1·5 | 0·970 |
| | $\overline{KE}$ | 1·5 | 0·970 |
| | $APE'$ | 0·042 | 1·000 |
| | $KE'$ | 0·054 | 1·000 |

was presented which combined semi-implicit and leapfrog time stepping for the solution of the barotropic and baroclinic modes respectively.

From the comparison of the energetics of the numerical and analytical solutions it was shown that the numerical scheme is convergent. However, at spatial resolutions lower than about 30 × 30 density grid points the barotropic mode of the numerical solution gets out of phase with that of the analytical solution, substantially worsening the agreement. In contrast, the agreement between the numerical baroclinic energetics and those of the analytical solution were less susceptible to decreasing spatial resolution; this is attributed to a far better temporal resolution of the baroclinic period than for the barotropic period.

Increasing the time step fivefold for the 50 × 50 grid caused the agreement between the numerical results and the analytical solution for the barotropic energetics to worsen substantially, without a corresponding decrease in the agreement for the baroclinic energetics. A linear stability analysis showed that the dispersive nature of the semi-implicit scheme was responsible for this behaviour.

In conclusion, the analytical solution presented herein is a useful validation tool for numerical shallow water models. It should be applied amongst a test suite of such validation tools before using

 

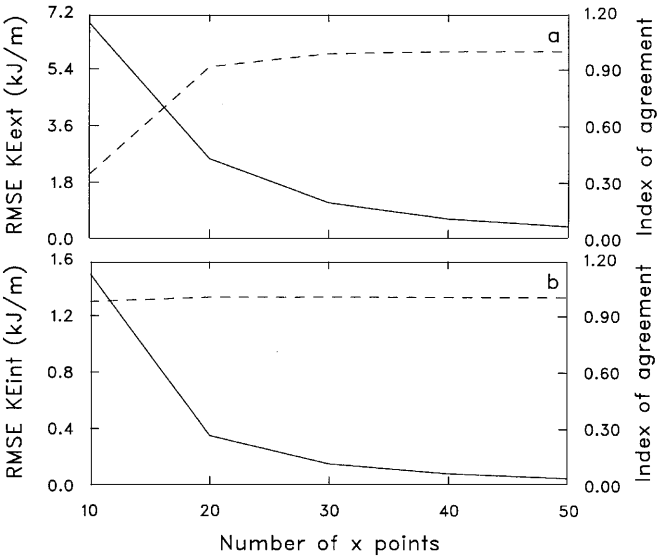


Figure 5. RMS error (RMSE, full line) and index of agreement (broken line) of comparison of numerical *APE* results with analytical solution for several grid sizes (as number of density points in *x*-direction): a, barotropic mode (APEext = $\overline{APE}$); b, baroclinic mode (APEint = *APE′*)

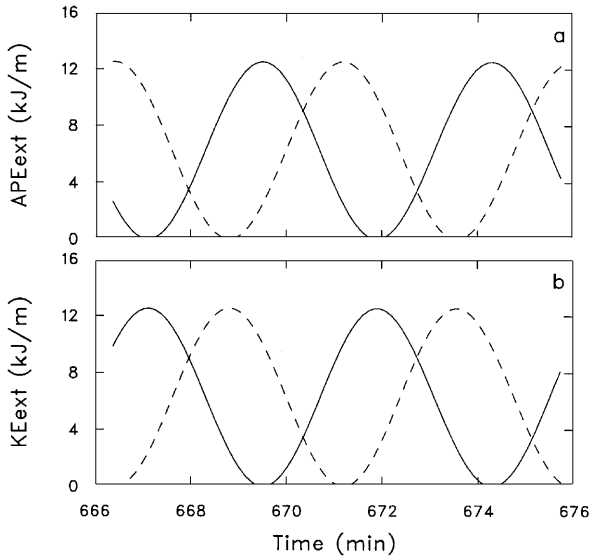


Figure 6. Energetics of analytical (broken line) and 10 × 10 grid numerical (full line) solutions for last barotropic seiche period during 'long' run: a, available potential energy of barotropic mode (APEext = $\overline{APE}$); b, kinetic energy (KEext = $\overline{KE}$)

 

such numerical models to simulate the more realistic geophysical flows encountered in lakes, bays, harbours and semi-enclosed seas under stratified conditions.

ACKNOWLEDGEMENTS

The first author would like to thank John Klinck for providing the analytical solution to the baroclinic mode and for his early idea for the numerical model, and also Eileen Hofmann for her support while initial ideas for this study germinated.

We would like to also acknowledge the comments of an anonymous reviewer, whose suggestions greatly strengthened this paper.

This study was begun with support from the Texas Engineering Experiment Station, Grant 32125B, and completed with support from the Department of Energy to the Lawrence Livermore National Laboratory under contract W-7405-ENG-48. This support is gratefully acknowledged.

## APPENDIX

To show that the semi-implicit solution of the barotropic mode of the numerical model leads to numerical dispersion, a linear stability analysis is made of equations (40) and (41). Denoting the imaginary number as 'i', using $j$ for the horizontal index, and substituting $U_i^n = \hat{U}^n e^{ij\alpha}$ and $\eta_i^n = \hat{\eta}^n e^{ij\alpha}$ into equations (40) and (41), then dividing through by $e^{i\alpha}$ gives

$$\hat{U}^{n+1} - \hat{U}^{n+1} = -\frac{c_o^2 \Delta t}{\Delta x} i \sin\left(\frac{\alpha}{2}\right)(\hat{\eta}^{n+1} + \hat{\eta}^{n-1}), \tag{50}$$

$$\hat{\eta}^{n+1} - \hat{\eta}^{n-1} = -\frac{\Delta t}{\Delta x} i \sin\left(\frac{\alpha}{2}\right)(\hat{U}^{n+1} + \hat{U}^{n-1}), \tag{51}$$

where use has been made of the identity $e^{i\alpha/2} - e^{-i\alpha/2} = 2i \sin(\alpha/2)$.

To eliminate $\hat{\eta}$ from equations (50) and (51), the time level $n$ equation of equation (50) is subtracted from its time level $n+2$ equation. The resulting three-time-level expression for $\hat{U}$ contains term involving $\hat{\eta}^{n+2} - \hat{\eta}^{n-2}$, which can be obtained by adding equation (51) at time level $n+2$ to its time level $n$ equation. Substituting the resulting expression for $\hat{\eta}^{n+2} - \hat{\eta}^{n-2}$ into the three-time level expression for $\hat{U}$ results in

$$(1+\gamma^2)\hat{U}^{n+2} - 2(1-\gamma^2)\hat{U}^n + (1+\gamma^2)\hat{U}^{n-2} = 0, \tag{52}$$

where $\gamma^2 = {C_r}^2 \sin^2(\alpha/2)$, with $Cr = c_o \Delta t/\Delta x$ being the Courant number.

The amplification of $\hat{U}$ as it steps forwards in time from time level $n$ to $n+2$ can be expressed as $\hat{U}^{n+2} = A\hat{U}^n$, where $A$ is the amplification factor. With this definition of $A$, equation (52) can be rewritten as a quadratic in $A$:

$$A^2 - \frac{2(1-\gamma^2)}{1+\gamma^2}A + 1 = 0. \tag{53}$$

Thus the amplification factor for the semi-implicit scheme is

$$A = \frac{1-\gamma^2 \pm 2i\gamma}{1+\gamma^2}. \tag{54}$$

The modulus of this amplification factor is $|A|^2 = 1$, so the semi-implicit scheme is unconditionally stable.

Of more interest to the analysis of the present results, however, is the phase shift of the numerical scheme. One way to evaluate the phase of the numerical scheme is to use Leenderste's [9] concept of

 

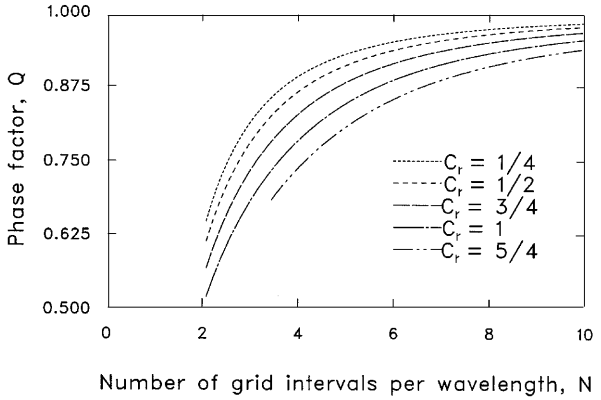


Figure 7. Phase factor ($Q$) of semi-implicit scheme versus number of grid intervals per wavelength ($N = 2\pi/\alpha$) for five values of Courant number: $Cr = 1/4$ (a), $1/2$ (b), $3/4$ (c), 1 (d) and $5/4$ above $N = \pi/\sin^{-1}(1/Cr) \approx 3{\cdot}39$ because of a discontinuity in $Q$ at that point when $Cr^2 \sin(\alpha/2) = 1$

the phase factor $Q$. The phase factor is defined as the ratio of the numerical phase to the analytical phase. Thus the numerical scheme is too fast if $Q > 1$ and too slow (i.e. dispersive) if $Q < 1$. For the present scheme,

$$Q = \frac{\tan^{-1}[2\gamma/(1-\gamma^2)]}{\alpha Cr}. \tag{55}$$

As shown for five values of the Courant number in Figure 7, $Q < 1$ for the present scheme, thereby illustrating that the present scheme is dispersive.

## REFERENCES

1. D. R. Lynch and C. B. Officer, 'Analytical test cases for three-dimensional hydrodynamical models', *Int. j. numer methods fluids*, **5**, 529–543 (1985).
2. G. Neumann and W. J. Pierson, *Principles of Physical Oceanography*, Prentice-Hall, Englewood Cliffs, NY, 1966.
3. A. E. Gill, *Atmosphere–Ocean Dynamics*, Academic, Orlando, FL, 1982.
4. L. H. Thomas 'Elliptic problems in linear difference equations over a network', *Watson Sci. Comput. Lab. Rep.*, Columbia University, NY, 1949.
5. G. P. Livingston, 'Distribution of the crustacean zooplankton in a subtropical estuarine system: implications for the predator–prey interactin between the primary and secondary consumers', *Ph.D Dissertation*, Texas A&M University, College Station, TX, 1981.
6. C. J. Wilmott, 'On the validation of models', *Phys. Geogr.*, **2**, 184–189 (1981).
7. P. D. Killworth, 'A note on smoothing techniques for leapfrog time-integration schemes', *Ocean Model.*, **60**, 5–8 (1984).
8. D. K. Lilly, 'On the computational stability of numerical solutions of time-dependent non-linear geophysical fluid dynamics problems', *Mon. Weather Rev.*, **93**, 11–26 (1965).
9. J. J. Leenderste, 'Aspects of a computational model for long-period water-wave propagation', *Mem RM-5294-PR*, Rand Corp., Santa Monica, CA, 1967.

 